applied sciences

MDPI

Article

Studies regarding the Use of Pneumatic Muscles in Precise Positioning Systems

Ioana Mădălina Petre

Department of Industrial Engineering and Management, Transilvania University of Brasov, 500036 Brasov, Romania; ioana.petre@unitbv.ro; Tel.: +40-268-477113

Abstract: The paper presents the methods and results of an experimental study that highlights the behavior of a pneumatic actuator under different pressures and with different loads applied. One important challenge that occurs in the application of pneumatic muscles is the phenomenon of hysteresis, which causes a nonlinear relationship between the input–output values. The aim of this study is to identify the occurrence of hysteresis in the operation of a small pneumatic muscle in different conditions. Thus, different loads are attached to the free end of a pneumatic muscle and different successive pressures are applied in order to examine the hysteresis of the contraction ratio when the muscle is inflated and then deflated. The obtained equations that describe the relationship between the input pressure and the axial contraction are significant for reaching a high-performance position control. In this regard, the article proposes a solution to increase positioning accuracy based on pressure control using a proportional pressure regulator and a programmable logic controller.

Keywords: pneumatic muscle; hysteresis; axial contraction; positioning systems

Citation: Petre, I.M. Studies regarding the Use of Pneumatic Muscles in Precise Positioning Systems. *Appl. Sci.* **2021**, *11*, 9855. https://doi.org/10.3390/app11219855

Academic Editor: Francisco Cavas Martínez

Received: 29 September 2021
Accepted: 20 October 2021
Published: 21 October 2021

1. Introduction

Nowadays, the use of pneumatic muscles is more and more common due to the advantages they have. A pneumatic muscle actuator (PMA) is a flexible tube made of an aramid fiber-reinforced rubber composite material. The elastomer is a chloroprene rubber and forms a matrix that integrates a 3D mesh of inelastic aramid fibers laid out in a diamond pattern. The working principle of a pneumatic muscle is correlated to its construction. Depending on the internal pressure applied to the pneumatic muscle, it increases in diameter and decreases in length.

The development of the pneumatic muscle is correlated to the necessity of obtaining alternatives for actuators, such as a simple or diaphragm cylinder, especially in the case of large dimensions, which involves higher weight and difficulties in stroke controlling. Even if the first mention of an artificial muscle was in 1930, when the Russian inventor S. Garasiev developed the pneumatic muscle [1], interest in these types of actuators increased, and many other types have appeared. In 2002, the company Festo submitted a patent for "Actuating means", a braided pneumatic muscle with robust end-fittings that allow it to be easily commercialized [2]. Later, the companies Shadow Robot Company and Merlin Systems Corporation produced braided pneumatic muscles on a commercial scale [3].

The applications of the pneumatic muscle are mostly found in industrial and medical domains such as industrial manipulators [4,5], robotic arms [6,7], and assistive devices for rehabilitation [8–11].

Pneumatic muscle actuators have numerous strengths, such as low weight, low workspace requirement, high flexibility to construct [8,12], adaptable installation possibilities, minimum consumption of compressed air, accessibility of different measurements, low cost, and being safe for human use [8,13]. These strengths are why it is recommended to be used as an actuator instead of electrical or hydraulic ones.

A weakness is the nonlinearity caused by the elastic, viscous properties of the inner rubber tube, the compressibility of air, and the structure of the complex behavior of the PMA outer covering [12].

Control accuracy of the pneumatic muscle depends on its behaviors in functioning as inelastic (namely hysteresis) or mechanical.

Paper [14] focused on the coupled deformation–diffusion response of fiber-reinforced polymeric gels based on the existence of the embedded fibers in a swellable polymer matrix, leading to anisotropy in the overall behavior. In [15], an experimental characterization and continuum modeling of inelasticity in filled rubber-like materials was presented. The results showed that the viscous stiffness exhibited strain-stiffening behavior during loading/unloading, and that stress-softening while experiencing a successive stretch did not affect the non-equilibrium behavior.

Wang and Chester [16] developed a thermo-mechanically coupled large deformation constitutive model that quantitatively captures thermal recovery of the stretch-induced stress softening (Mullins effect) of elastomeric materials. Furthermore, Wang et al. [17] showed that viscoelasticity provides stabilization that delays the onset of instability under monotonic loading and may fully suppress instabilities under sufficiently fast cyclic loading, which may be desirable for many applications.

Hysteresis, as a common nonlinear phenomenon that appears in numerous systems, has been studied by numerous researchers. Studies were made on piezoelectric-actuated stages [18,19], magnetostrictive actuators [20,21], and pneumatic actuators [22–24].

In the case of pneumatic muscles, the analysis of force/length hysteresis or pressure/length hysteresis can be made in an isobaric or isotonic contraction test [4,25]. Some modeling methods have been proposed for establishing the hysteresis phenomenon in the pneumatic muscle actuator analysis.

The Maxwell-slip model [26] was used as a lumped-parametric quasi-static model proposed to capture the force/length hysteresis of a PMA. The proposed model describes the force/length hysteresis at different excitation intervals and with different internal pressures.

The Jiles–Artherton model [27] was used to establish the pneumatic muscle hysteresis model and its compensation control. The needed parameters of the model were identified using adaptive weighted particle swarm optimization.

T. Kosaki and M. Sano used the Preisach model to describe hysteresis nonlinearity in the relationship between the contraction and internal pressure of pneumatic muscle [28]. The model was also used for the control of a parallel manipulator driven by three pneumatic muscles. In [29], the proposed technique used the dynamic Preisach model and adaptively tuned the parameters of the model by recursive parameter estimation if the distortion occurred due to speed variations.

In [30], the generalized Prandtl–Iskhlinskii model was used for characterizing the hysteresis of a pneumatic muscle. The model could accurately describe asymmetric hysteresis and had high accuracy in the trajectory tracking of the pneumatic artificial muscle.

The research conducted to date in the field of modeling the hysteresis of a pneumatic muscle highlights the conclusion that the models are not suitable for generalization. They were developed by a certain type of muscle which was the object of the research. The difficulty of identifying a generalized model for pneumatic muscle hysteresis is due to the "soft" character of the artificial muscle, combining elastomer physics with textile physics [31].

Electro-pneumatic systems are among the most widely used systems when it comes to areas of activity with special environmental conditions due to the clean working agent (air) and their advantages, high working forces and speeds.

Even if their positioning accuracy can still be improved, pneumatic positioning systems are an alternative to electro-mechanical ones as they are reliable and long-lasting.

Most pneumatic positioning systems, which combine control valves, cylinders, and position transducers, rely on directional airflow control to control positioning. This type of system achieves precise positioning with the help of a rigorous control of the air flow. In this situation,

the air loss resulting from the impossibility of a perfect seal between the movable element (rod or piston) and the fixed one (cylinder liner) must be taken into account.

A positioning system must be able to reach and maintain the required position anywhere along the length of the stroke. Based on the well-known presence of hysteresis in pneumatic muscle function, this paper presents the methods and results of an experimental study that highlights the behavior of a pneumatic actuator under different pressures and with different loads applied. Positioning accuracy is an imposed condition in many applications but is limited in the case of using pneumatic muscles due to their inherent nonlinearity and hysteresis. The aim of this paper is to model the axial contraction/pressure hysteresis of a small pneumatic muscle and to establish an accurate positioning control.

The proposed method of increasing positioning accuracy is based on pressure control using a proportional pressure regulator and a Programmable Logic Controller (PLC).

The structure of the paper includes a section that describes the materials and methods of the research. The experimental setup and the used components, and the method used for the experiment, are presented. The third section of the paper presents several experiments and results for determining the hysteretic behavior of a pneumatic muscle of 10 mm diameter and 100 mm length. In this section, some polynomial regression functions are developed, which can be used to configure the pneumatic actuation system. In the last section of the paper, the conclusions of the research and future directions are presented.

2. Materials and Methods

2.1. Components of Experimental Setup

The experimental setup used for determining the relation between the axial contraction (Δl) of the pneumatic muscle and the internal pressure (p) applied gradually consisted of several components, as presented in the Figure 1.

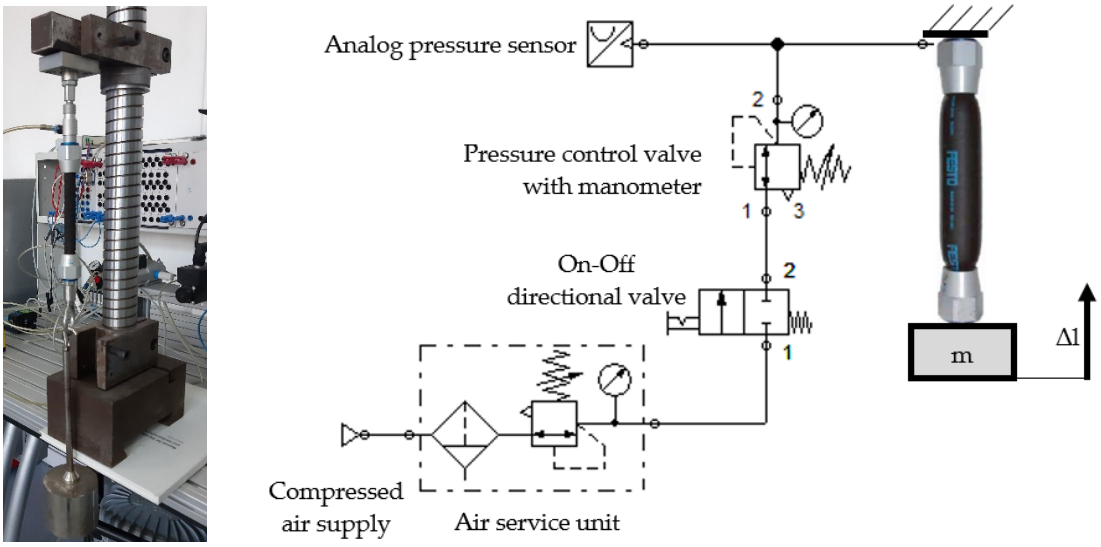

(**a**) (**b**)

Figure 1. Experimental setup. (**a**) Picture; (**b**) control diagram.

The investigated pneumatic actuated muscle (Figure 2a) is manufactured by FESTO, Germany (MAS-10-N-100-AA-MCFK), and its characteristics are presented in Table 1.

(**a**) (**b**)

Figure 2. Pneumatic muscle. (**a**) Picture; (**b**) working diagram.

Table 1. Characteristics of the investigated pneumatic muscle.

Parameter	Value
Length	100 mm
Diameter	10 mm
Maximum working pressure	8 bar
Axial contraction	Max. 20 mm
Force that can be generated	Max. 492 N

The control diagram is presented in Figure 1b. The pressure of the compressed air delivered by the compressor was set by the pressure control valve with a manometer. The value of the compressed air pressure was read at the display of the analog pressure sensor. The resulted displacement of the muscle was measured after each experiment.

The components of the experimental stand were from Festo Ag & Co., and their main characteristics are presented in the table below (Table 2):

Table 2. Components and characteristics of the experimental setup.

Component	Characteristics
Pressure control valve with manometer	The pressure gauge displays the pressure in the pneumatic circuit within 0–10 bar
The analog pressure sensor	Power supply 15–30 V dc Analog output 0–10 V dc Pressure measuring range 0–10 bar
On-off directional valve	Pressure range 0–8 bar Maximum flow: 60 L/min (ANR)
Displacement sensor	Linear potentiometer, 200 mm stroke

2.2. Pneumatic Muscle Principle

The pneumatic muscle is a system that involves the contraction of a membrane, and works on a principle similar to that of human muscle. It ensures movement by changing its geometric shape when placed under pressure. Consisting of an elastomer tube reinforced with aramid fibers (synthetic fibers), the pneumatic muscle contracts rapidly and exerts pulling forces when supplied with pressurized air. As compressed air enters the muscle, a traction force is developed that works along the longitudinal axis, and the muscle is shortened in proportion to the increase in the internal pressure. The contraction reduces the length of the muscle by up to 25% of the initial value in the unloaded state. The pneumatic muscle achieves a maximum force as soon as the contraction begins, with the developed force being zero at the end of the stroke. The working diagram of the pneumatic muscle can be seen in Figure 2b.

According to [32], pneumatic muscles are able to reproduce movements that closely mimic the kinematics, speed, strength, and refinement of natural muscles.

The characteristics of pneumatic actuators have been investigated by many researchers, and some research findings have been achieved. The dynamic model was proposed in [33],

which included the processes of contraction upon inflation and deflation of a pneumatic actuator. In addition, the best fitting parameters were determined by utilizing the least square linear regression method in [34] to depict the hysteresis phenomenon. Similar work can also be found in [35].

Due to their construction, pneumatic muscles develop a nonlinear and hysteretic behavior. An example is the hysteresis of axial contraction–pressure dependence, which is presented in this research.

The occurrence of the hysteresis phenomenon is well-known for pneumatic muscles, therefore, tracking the control performance of it is difficult.

Some possible causes of hysteresis in the functioning of pneumatic muscles are friction between fibers, friction between fibers and rubber tube, conical deformation of the rubber tube at its end, and the stretching of rubber tube due to increased volume [26,31].

The actuation of an artificial muscle is made by means of compressed air, which is introduced or extracted from it. Although it is possible to design a muscle to function in depression, in most cases, these actuators function in overpressure, according to [1] and [32]. This is because the compressed air supply is easier to achieve, and, on the other hand, much more energy can be transmitted through overpressure than through depression.

Feeding a pneumatic muscle with compressed air allows it to move a load in a certain direction. Once the air supply is interrupted (it is removed from the muscles), the load is moved in the opposite direction (Figure 2b).

The mode of operation of a pneumatic muscle can be observed by performing two experiments (Figure 3), according to [32,36]. In both cases, the muscle is fixed at one end and a mass load (M) is attached to the other end.

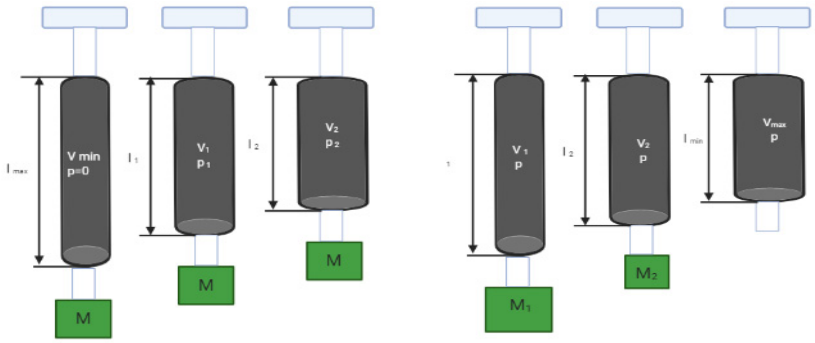

Figure 3. Operating mode at (**a**) constant load (M); (**b**) constant pressure (p).

For the first experiment (Figure 3a), the mass (M) is constant and the initial supply pressure is zero. At zero pressure, the volume of the muscle is minimal (V_{min}) and its length is maximal (l_{max}). If the muscle is fed to the pressure (p_1), it will begin to expand in diameter and, at the same time, will develop a pulling force, lifting the load (M). The muscle volume will reach the value V_1 and its length will become l_1. Increasing the pressure to p_2 will continue this process.

From this experiment, two basic rules can be deduced, according to [32]:

(1) A pneumatic muscle is shortened by increasing its radial dimensions;

(2) The length of the muscle will decrease as the pressure increases, the applied load being constant.

From the second experiment, presented in Figure 3b, two other rules arise. The pressure is maintained at a constant value (p), while the mass attached to the free end is diminished. In this case, the muscle will expand in the radial direction and shorten. If the load is completely removed, the expanding in the radial direction is at its maximum and the length will reach its minimum value, l_{min}.

As result, it means that:

(3) A muscle at a constant pressure will shorten if its load is reduced;
(4) Its axial contraction has an upper limit over which no force develops.
From both experiments presented above, another rule can be deduced:
(5) For each pair of pressure–load, a pneumatic muscle has an equilibrium length.

This behavior differs from that of a pneumatic cylinder; a cylinder develops a force that depends only on the pressure and the surface of the piston. Therefore, at a constant pressure, the force will be constant, regardless of the displacement performed.

The presented research applied the first operating mode (Figure 3a) with a constant load and increased the pressure from 0 to 6 bar. There are three situations considered for the experiment: without a load at the free end of the muscle, with a 2.55 kg load, and with a 4.55 kg load.

2.3. Method

The aim of this study was to identify the occurrence of hysteresis in the operation of a small pneumatic muscle in different conditions. The experiment to find the hysteresis of the pneumatic muscle was performed as follows:

1. An air pressure is applied to the actuator from 0 to 6 bar by 0.5 bar steps. There is no load applied to the free end of the muscle (M = 0 kg);
2. At each step, the length of the PMA is measured;
3. A 2.55 kg load is attached to the free end of the muscle;
4. Steps 1 and 2 are repeated;
5. A 4.55 kg load is attached to the free end of the muscle;
6. Steps 1 and 2 are repeated;
7. The obtained data is processed.

After each pressure level was reached, and prior to performing the measurement, a minute of rest was allowed in order for the muscle length to stabilize. The measurements were repeated five times, and five cycles of inflation/deflation with air of the pneumatic muscle were conducted. The contraction was measured using a linear potentiometer, 200 mm stroke code 167090 (produced by Festo AG & Co., Esslingen, Germany).

The axial contraction of the pneumatic muscle decreases while the applied pressure is raised. Even if the contraction ratio (ε) is specified as being 25% for the considered muscle, it is not fixed for all actuators and it depends on the type of inner rubber tube, the diameter of the PMA, and the maximum diameter of the braided sleeve [37].

The study in [37] also confirms that the contraction ratio of a pneumatic muscle depends on the stiffness and diameter of the actuator and is not fixed.

In [38], the hysteresis curves that describe the radial and axial dimensional modifications of a small pneumatic muscle, as well as the variation of the developed forces for different feed pressures, were presented.

3. Results

The experimental research and the obtained results followed two directions. The first direction aimed to prove the existence of the hysteresis phenomenon at the analyzed muscle. Therefore, the dependence between pressure and the axial contraction was developed. The input pressure variation returned different values for the axial contraction of the muscle. Based on those values, several equations were found. The purpose of the second direction of research was to determine the pressure depending on the axial contraction of the pneumatic muscle in order to develop several equations used for the PLC.

3.1. Evaluation of Hysteresis

The results are presented in the following lines, considering the three situations of different loads applied to the free end of the muscle.

3.1.1. Evaluation of the Hysteresis for the Case of No Load Applied

For the situation of no load applied to the free end of the muscle, the measurement data are presented in Table 3. The measured data are plotted in Figure 4, showing the evolution of axial contraction versus applied pressure.

Table 3. Muscle axial contraction for zero external load.

Pressure [bar]		Axial Contraction [mm]					Arithmetic Mean	Standard Deviation
		1	2	3	4	5		
Inflation	0	0	0	0	0	0	0	0
	0.5	0.4	0.45	0.35	0.47	0.38	0.41	0.04427
	1	0.9	1	1	1	1.1	1	0.06325
	1.5	1.5	1.7	1.65	1.7	1.45	1.6	0.10488
	2	2.7	2.4	2.9	2.5	3	2.7	0.22804
	2.5	3.3	4	3.6	3.7	3.9	3.7	0.24495
	3	4.8	4.9	5.4	5.4	5.5	5.2	0.28983
	3.5	7	7.2	7.1	6.9	7.3	7.1	0.14142
	4	8.4	8.5	8.7	8.6	8.8	8.6	0.14142
	4.5	10	10.3	10.3	9.9	10.4	10.18	0.19391
	5	11.9	11.9	12.1	12	11.7	11.92	0.13266
	5.5	12.7	12.8	12.8	13	12.7	12.8	0.10954
Deflation	6	15	14.9	15.1	15.2	15.3	15.1	0.14142
	5.5	14.8	14.5	14.2	14.3	14.7	14.5	0.22803
	5	13.8	14	14.1	13.7	13.9	13.9	0.14142
	4.5	12.7	12.65	12.45	12.8	12.9	12.7	0.15165
	4	11.7	11.6	11.4	11.6	11.7	11.6	0.10954
	3.5	10.5	10.4	10.35	10.4	10.3	10.39	0.06633
	3	8	8.2	8.4	8.3	8.2	8.22	0.13266
	2.5	6.2	6.4	6.3	6	6.1	6.2	0.14142
	2	4.7	4.6	4.3	4.7	4.7	4.6	0.15491
	1.5	2.9	3.4	3.4	3.1	3.2	3.2	0.18973
	1	1.6	1.9	2.1	2	1.9	1.9	0.16733
	0.5	0.9	0.8	1.1	1	1.2	1	0.14142
	0	0.2	0.3	0.4	0.35	0.3	0.31	0.06633

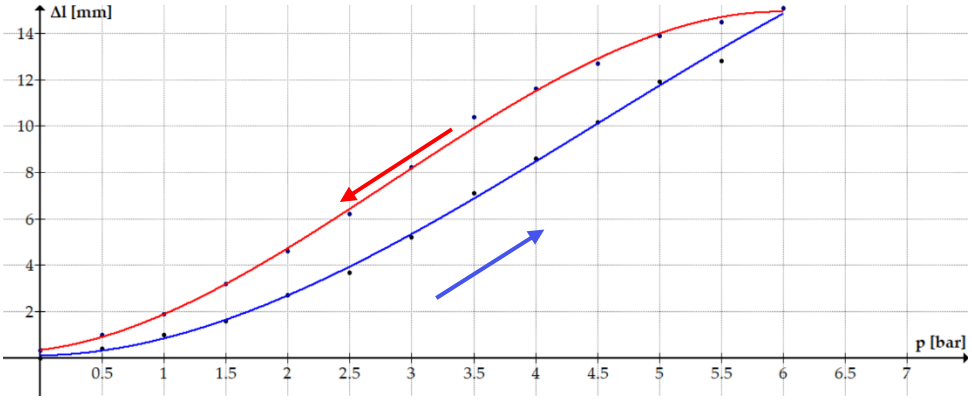

Figure 4. Evolution of the axial contraction versus pressure (no load).

For each value of applied pressure, the results show that the axial contraction of the muscle at inflation is different from the obtained value at deflation. The bottom line represents the axial contraction while the muscle is being inflated, the top line represents the displacement during deflation.

At deflation, the values are higher than the values obtained at inflation, the maximum difference between them being 3.29 mm in the middle pressure area (3.5 bar).

The arithmetic mean and the standard deviation illustrate the statistical dispersion of the measured values. The values of the standard deviation are noticeably small, close to zero, and indicate a low uncertainty of the measurements.

Figure 5 presents the third-degree polynomial regression function, which best fits the obtained results at inflation. The red line represents the evolution of the measured values, and the colored zone represents the range of confidence.

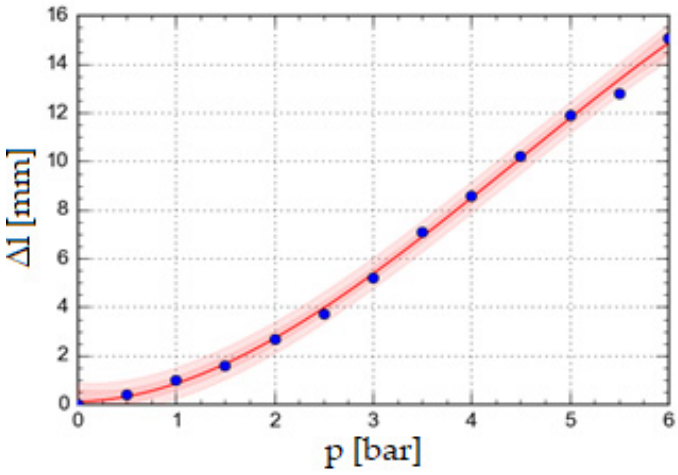

Figure 5. Polynomial regression curve: inflation.

The polynomial regression that best fits the measured values for inflation is one of a third degree, as seen in Equation (1):

$$\Delta l_{inflation} = 0.096 + 0.079 \cdot p + 0.718 \cdot p^2 - 0.053 \cdot p^3 \quad (1)$$

The parameters of the regression were found using a specialized software, the Curve Expert Professional v. 2.7, and based on the measured values. The correlation coefficient (r) is 0.999 and the coefficient of determination (r^2) is 0.998. Those values validate the function.

In Figure 6, the polynomial regression is presented, which best fits the obtained results at deflation.

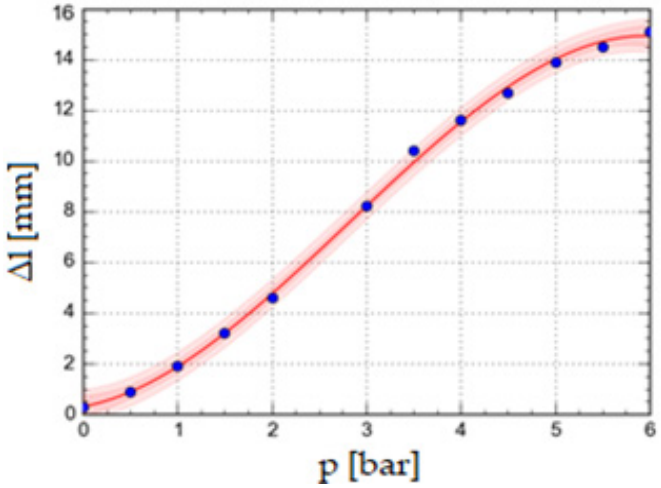

Figure 6. Polynomial regression: deflation.

The polynomial regression that best fits the measured values at deflation is, according to Curve Expert Professional v. 2.7 software:

$$\Delta l_{deflation} = 0.296 + 0.684 \cdot p + 1.005 \cdot p^2 - 0.118 \cdot p^3 \quad (2)$$

The correlation coefficient (r) is 0.999 and the coefficient of determination (r^2) is 0.998. These values confirm that this function describes the evolution of axial contraction versus pressure at deflation with high fidelity.

3.1.2. Evaluation of Hysteresis for the Case of a 2.55 kg Load Applied

For the situation of a mass of 2.55 kg load applied to the free end of the muscle, the measurement data are presented in Table 4 and Figure 7.

Table 4. Muscle axial contraction for a 2.55 kg external load.

Pressure [bar]		Length [mm]					Arithmetic Mean	Standard Deviation
		1	2	3	4	5		
Inflation	0	0	0	0	0	0	0	0
	0.5	0.2	0.3	0.4	0.2	0.4	0.3	0.08944
	1	0.9	1.1	1.2	1	1.3	1.1	0.14142
	1.5	1.5	1.6	1.4	1.6	1.4	1.5	0.08944
	2	2.3	2.5	2.4	2.2	2.6	2.4	0.14142
	2.5	3.4	3.5	3.6	3.4	3.6	3.5	0.08944
	3	5	5.1	5.2	5.2	5	5.1	0.08944
	3.5	6.9	7	7.1	6.8	6.8	6.92	0.11662
	4	8.3	8.5	8.4	8.3	8.4	8.38	0.07483
	4.5	9.6	9.7	9.5	9.4	9.7	9.58	0.11662
	5	11.5	11.8	11.7	11.6	11.5	11.62	0.11662
	5.5	12.4	12.6	12.3	12.5	12.6	12.48	0.11662
Deflation	6	14.7	14.8	14.9	14.7	14.8	14.78	0.07483
	5.5	14.7	14.7	14.4	14.7	14	14.5	0.27568
	5	13.6	13.7	13.5	13.5	13.7	13.6	0.08944
	4.5	12.4	12.5	12.3	12.4	12.4	12.4	0.06325
	4	11	10.8	10.8	10.9	11	10.9	0.08944
	3.5	9.5	9.3	9.4	9.2	9.6	9.4	0.14142
	3	7.4	7.5	7.6	7.5	7.5	7.5	0.06325
	2.5	5.5	5.8	5.6	5.5	5.6	5.6	0.10954
	2	4	4.4	4.2	4.3	4.1	4.2	0.14142
	1.5	2.5	2.7	2.8	2.9	2.6	2.7	0.14142
	1	1.8	1.7	1.7	1.9	1.9	1.8	0.08944
	0.5	0.8	1	1	0.8	0.9	0.9	0.08944
	0	0.2	0.1	0.4	0.4	0.4	0.3	0.12649

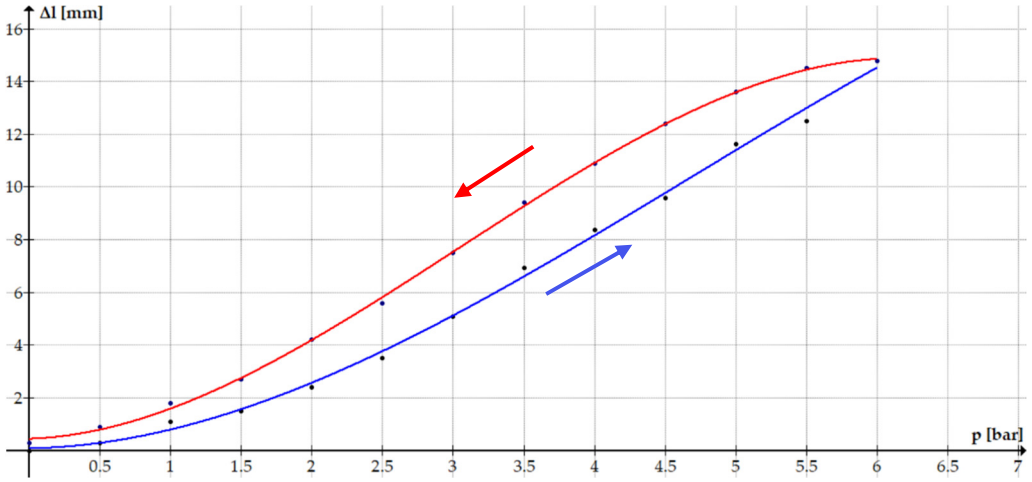

Figure 7. Evolution of axial contraction versus pressure (M = 2.55 kg).

It can be observed that, in this case, and similar to previous values, the behavior of the inflated/deflated muscle is not linear. As seen in Figure 7, the inflating values and

evolution of axial contraction are plotted with a blue line and the deflating variation is represented with a red line. There is a distance between the obtained values, the maximum value between inflation and deflation being 2.82 mm at a pressure of 4.5 bar.

At inflation, with a 2.55 kg mass attached to the free end of the pneumatic muscle, the polynomial regression that best fits the measured data is presented in Equation (3) and for deflation in Equation (4). The evolution of these values can be seen in Figure 8.

$$\Delta l_{inflation} = 0.096 + 0.079 \cdot p + 0.718 \cdot p^2 - 0.053 \cdot p^3 \quad (3)$$

$$\Delta l_{deflation} = 0.439 + 0.180 \cdot p + 1.092 \cdot p^2 - 0.120 \cdot p^3 \quad (4)$$

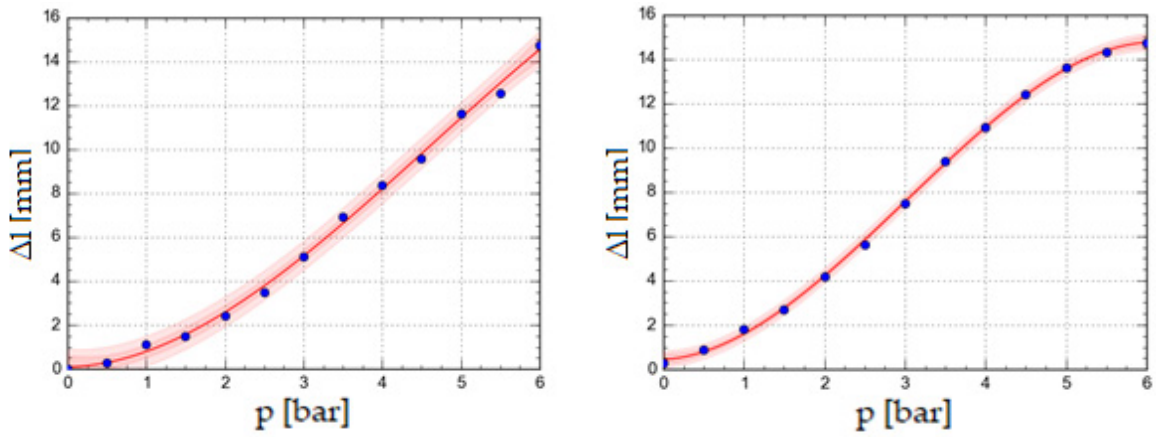

(**a**) (**b**)

Figure 8. Polynomial regression. (**a**) Inflation; (**b**) deflation.

For both regressions, the correlation coefficients ($r_{inflation} = 0.998$, $r_{deflation} = 0.999$) and the coefficients of determination ($r^2{}_{inflation} = 0.997$, $r^2{}_{deflation} = 0.999$) validate the functions developed in Equations (3) and (4).

3.1.3. Evaluation of Hysteresis for the Case of a 4.55 kg Load Applied

For the situation of a 4.55 kg load applied to the free end of the muscle, the measurement data are presented in Table 5 and Figure 9.

In this case, the values measured at the deflation of the muscle are higher than the values measured at inflation, the maximum distance between those being 2.4 mm at a pressure of 3.5 bar.

At inflation, with a 4.55 kg mass attached to the free end of the pneumatic muscle, the polynomial regression that best fits the measured data is presented in Equations (5) and (6). The evolution of these values and the 95% range of confidence can be seen in Figure 10.

$$\Delta l_{inflation} = 0.071 - 0.421 \cdot p + 0.786 \cdot p^2 - 0.055 \cdot p^3 \quad (5)$$

$$\Delta l_{deflation} = 0.270 + 0.005 \cdot p + 1.016 \cdot p^2 - 0.106 \cdot p^3 \quad (6)$$

The functions are validated by the correlation coefficient ($r = 0.999$), and by the coefficient of determination ($r^2 = 0.999$).

Table 5. Muscle axial contraction for a 4.55 kg external load.

Pressure [bar]		Length [mm]					Arithmetic Mean	Standard Deviation
		1	2	3	4	5		
Inflation	0	0	0	0	0	0	0	0
	0.5	0.2	0.1	0	0.1	0.1	0.1	0.06325
	1	0.5	0.4	0.4	0.7	0.5	0.5	0.10954
	1.5	0.9	1	1.1	1	1	1	0.06325
	2	1.7	2	1.9	1.9	2	1.9	0.10954
	2.5	2.9	3	3.1	3	3	3	0.06325
	3	4.4	4	4.7	4.6	4.3	4.4	0.24495
	3.5	5.7	5.8	5.9	5.8	5.8	5.8	0.06325
	4	7.6	7.7	7.8	7.5	7.4	7.6	0.14142
	4.5	9.5	9.7	9.8	9.7	9.8	9.7	0.10954
	5	11.4	11.2	11.5	11.2	11.2	11.3	0.12649
	5.5	12.7	12.9	12.7	12.8	12.9	12.8	0.08944
Deflation	6	14	14.1	13.9	14	14	14	0.06325
	5.5	13.4	13.4	13.2	13.2	13.3	13.3	0.08944
	5	12.5	12.3	12.3	12.4	12.5	12.4	0.08944
	4.5	11.4	11.3	11.5	11.3	11.5	11.4	0.08944
	4	9.9	9.8	9.8	9.7	9.8	9.8	0.06325
	3.5	8.1	8.3	8.2	8.1	8.3	8.2	0.08944
	3	6.4	6.6	6.4	6.6	6.5	6.5	0.08944
	2.5	4.6	4.7	5.1	4.9	4.7	4.8	0.17889
	2	3.5	3.6	3.3	3.7	3.4	3.5	0.14142
	1.5	2.3	2.4	1.9	2.3	2.1	2.2	0.17889
	1	1.2	1.6	1.4	1.7	1.1	1.4	0.22804
	0.5	0.5	0.4	0.5	0.7	0.4	0.5	0.10954
	0	0.2	0.1	0.3	0.2	0.2	0.2	0.06325

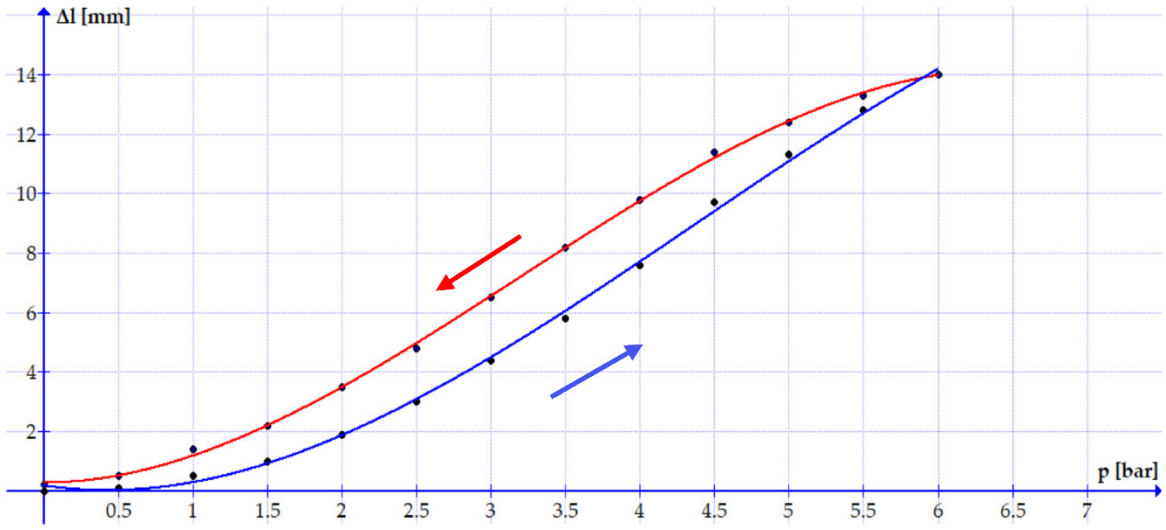

Figure 9. Evolution of the axial contraction versus pressure (M = 4.55 kg).

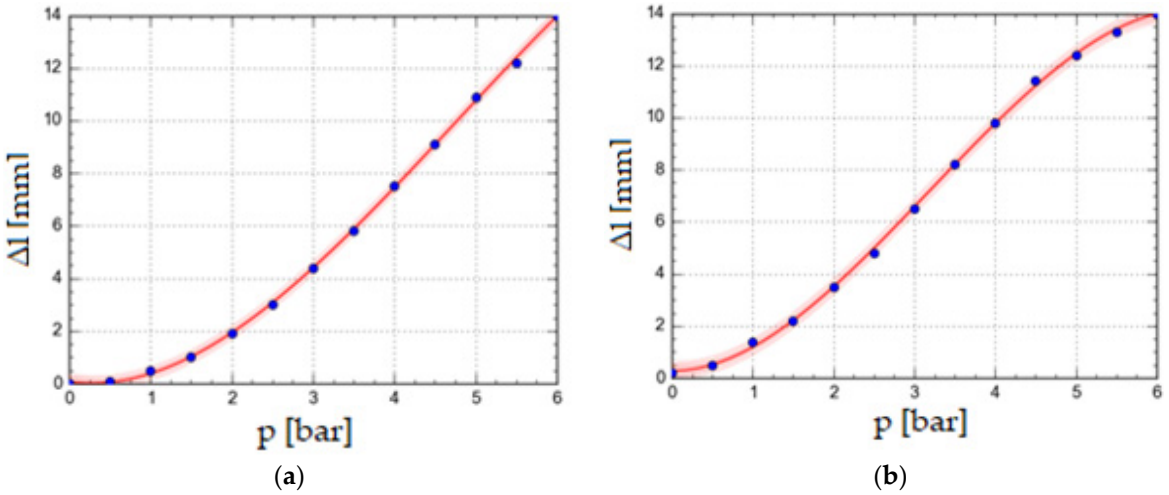

Figure 10. Polynomial regression. (**a**) Inflation; (**b**) deflation.

3.2. Evaluation of the Relation between the Axial Contraction and the Input Pressure

Of interest for the study of the positioning accuracy of the mechanical systems driven by the pneumatic muscles is the dependence of the pressure necessary for supplying these actuators on the size of the axial contraction that needs to be performed. In this regard, based on the measured values, a short analysis was made in order to deduce the relation between the input pressure and axial contraction. Thus, for the considered cases, the necessary pressures for obtaining some axial contraction were found. These can be seen in Table 6.

Table 6. Supply pressure values necessary for axial contraction of the muscle.

Axial Contraction [mm]	M = 0 kg p [bar]		M = 2.55 kg p [bar]		M = 4.55 kg p [bar]	
	Inflation	Deflation	Inflation	Deflation	Inflation	Deflation
2	1.66	1.24	1.88	1.16	1.43	1.38
4	2.54	1.78	2.72	1.95	2.91	2.18
6	3.16	2.43	3.25	2.64	3.49	2.84
8	3.86	2.96	3.90	3.19	4.07	3.47
10	4.53	3.4	4.62	3.72	4.59	4.10
12	4.94	4.28	5.14	4.33	5.19	4.80
14	5.71	4.98	5.85	5.19	5.96	5.93

In Figure 11, the evolution of the input air pressure versus pneumatic muscle axial contraction is presented. The dots represent the axial contraction values, and the lines represent the polynomial regression curves. For M = 0 kg, the functions that describe the input pressure evolution versus axial contraction at inflation and deflation are:

$$p_{inflation} = 0.001 \cdot \Delta l^3 - 0.028 \cdot \Delta l^2 + 0.565 \cdot \Delta l + 0.637 \quad (7)$$

$$p_{deflation} = 0.001 \cdot \Delta l^3 - 0.0172 \cdot \Delta l^2 + 0.376 \cdot \Delta l + 0.537 \quad (8)$$

The graphs for the 2.55 kg and 4.55 kg loads are shown in Figures 12 and 13.

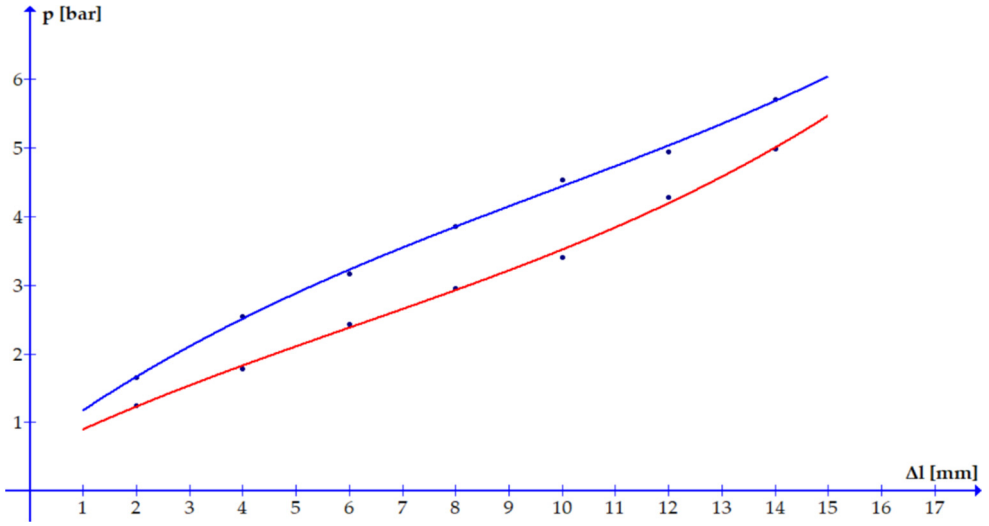

Figure 11. The evolution of the input pressure versus axial contraction (M = 0 kg).

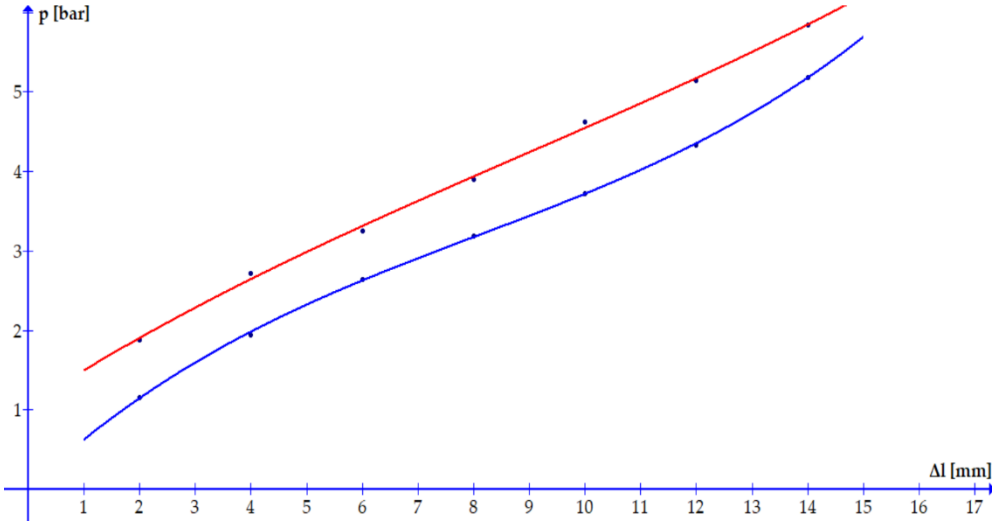

Figure 12. The evolution of the input pressure versus axial contraction (M = 2.55 kg).

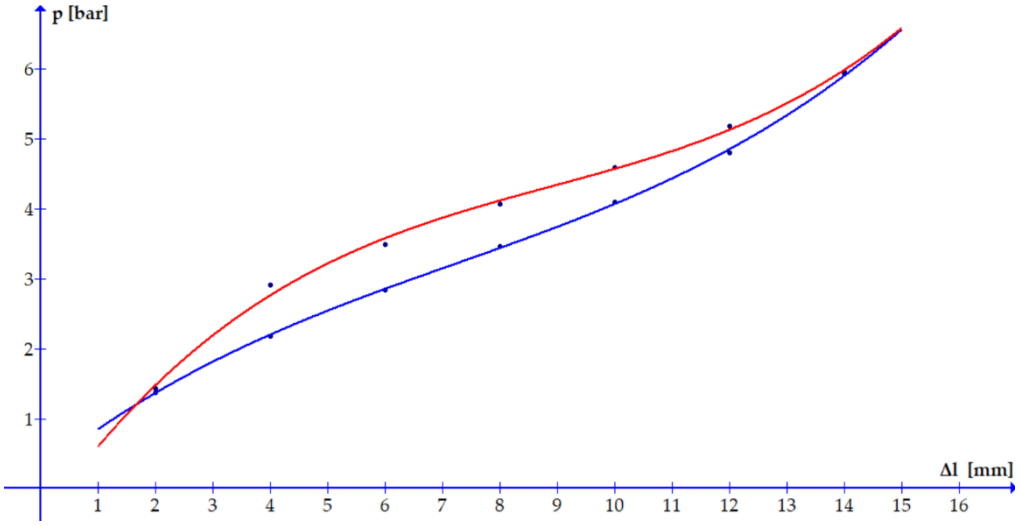

Figure 13. The evolution of the input pressure versus axial contraction (M = 4.55 kg).

The equations that describe the variation of the input pressure versus axial contractions for when a 2.55 kg load is applied to the free end of the muscle are as follows:

$$p_{inflation} = 0.001 \cdot \Delta l^3 - 0.016 \cdot \Delta l^2 + 0.452 \cdot \Delta l + 1.06 \quad (9)$$

$$p_{deflation} = 0.002 \cdot \Delta l^3 - 0.047 \cdot \Delta l^2 + 0.649 \cdot \Delta l + 0.024 \quad (10)$$

The equations that describe the variation of the input pressure versus axial contraction when a 4.55 kg load is applied to the free end of the muscle are presented in Equations (11) and (12). Those equations are validated by the coefficients of determination (R^2), which have the values of 0.9972 and 0.9996.

$$p_{inflation} = 0.003 \cdot \Delta l^3 - 0.106 \cdot \Delta l^2 + 1.168 \cdot \Delta l - 0.461 \quad (11)$$

$$p_{deflation} = 0.002 \cdot \Delta l^3 - 0.0503 \cdot \Delta l^2 + 0.653 \cdot \Delta l + 0.244 \quad (12)$$

In order to obtain precise and predictable contractions at the free end of the pneumatic muscle, Equations (7)–(12) must be known and used for control by means of a proportional pressure regulator of the pneumatic muscle supply. Figure 14 shows a control scheme that includes such a proportional pressure regulator.

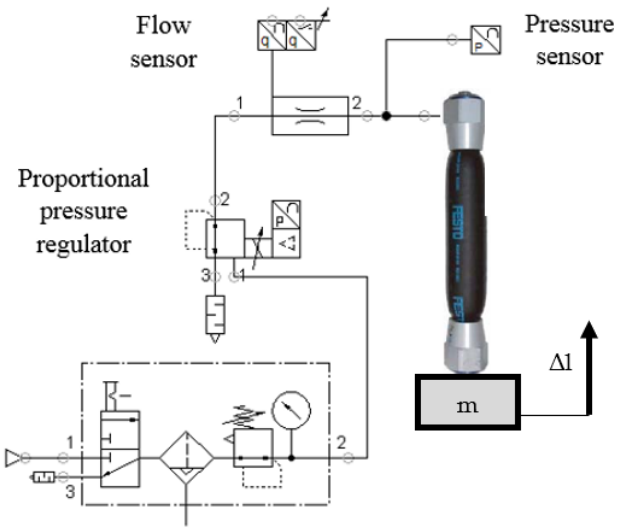

Figure 14. Supply pressure adjustment with a proportional pressure regulator.

Compressed air is fed to the muscle through an MPPES-3-1/4-6-010 proportional pressure regulator (produced by Festo AG & Co., Esslingen, Germany). This control diagram enables the slow and uniform charging of the pneumatic muscle without introducing shocks.

A specially developed computer programme based on the experimentally determined polynomial equations was loaded to a Programmable Logic Controller (PLC). The PLC sends an electric signal to the proportional pressure regulator, whose voltage is continuously modified according to the experimentally obtained polynomial function. This affects the desired variation of air pressure in the pneumatic muscle and, consequently, the desired contractions and forces [39].

Figure 15 shows an example of positioning an object with a mass of 2.55 kg using the control diagram proposed above. The red line shows the motion paths obtained under these conditions. The movement paths obtained using the diagram in Figure 1b is drawn in blue. It can be seen that the accuracy of positioning by controlling the pressure with the help of a proportional regulator is very good, with the proposed system offering a viable and efficient alternative.

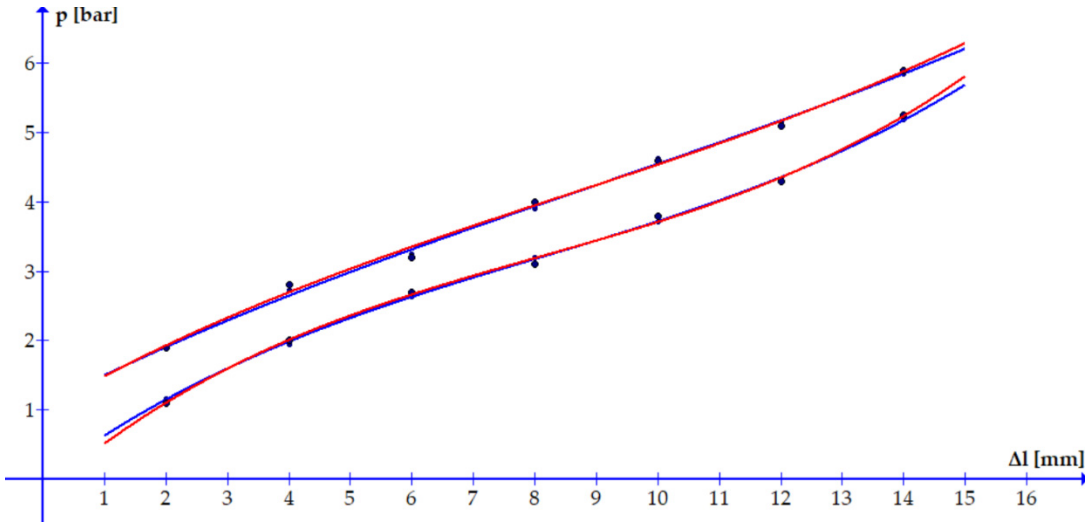

Figure 15. The motion curve of an object with a mass of 2.55 kg.

A significant disadvantage of the pneumatic muscles used for precise positioning systems is that, for each actuator, experiments must be performed, then it is necessary to determine the dependencies ($p = f\ (\Delta l)$) in both the inflation and the deflation phase. These relationships must then be loaded into the PLC.

The transposition into practice of the working method presented above, i.e., that of obtaining high positioning accuracies for work equipment actuated with pneumatic muscles, has been shown by the author in several previously published articles [40,41].

In [40], a rehabilitation equipment of the lower limb joints (hip, knee, and ankle) is presented. Its actuation is carried out with the help of a pneumatic muscle for which the hysteresis curves were experimentally determined. Based on these, the PLC was programmed, with the results obtained validating the used working method.

In [41], a hand joint rehabilitation equipment driven by a pneumatic muscle is described. Using the same working methodology, the results obtained confirmed its validity.

4. Conclusions

The conducted experiments highlighted the occurrence of the phenomenon of hysteresis during the inflation/deflation cycles of a pneumatic artificial muscle under different loads applied to the free end. The variation of the axial contraction depending on the pressure was described by several polynomials, developed based on experimental results. The relationship between axial contraction and the internal pressure of the muscle at inflation differs from the relationship determined at deflation. As seen in the experiments, the maximum contraction can be observed when the muscle is not loaded.

The obtained results revealed the hysteretic behavior of the studied pneumatic muscle. Hysteresis represents a map between the input and output variables which affect the control performance of the muscle. Therefore, hysteresis should be compensated by using an inverse model, such as an inverse block with the desired value of control variable at its input.

The obtained equations that describe the relationship between the input pressure and the axial contraction are significant for reaching a high-performance position control. In this regard, the article proposed a solution to increase positioning accuracy based on pressure control using a proportional pressure regulator and a PLC. The experimental results obtained confirm the possibility of accurately positioning the driven systems with the help of pneumatic muscles. The presented work methodology is specific to a certain working situation (range of applied pressures and external loads), it must be repeated for each application. Further research is to find a path for generalizing the outcomes obtained for other applications.

Funding: This research received no external funding.

Conflicts of Interest: The author declare no conflict of interest.

References

1. Marcinčin, J.; Palko, A. Negative pressure artificial muscle—An unconventional drive of robotic and handling systems. In *Transactions of the University of Košice*; Riecansky Science Publishing Co.: Košice, Slovakia, 1993; pp. 350–354.
2. Bergemann, D.; Lorenz, B.; Thallemer, A. Actuating means. U.S. Patent US6349746B1, 26 February 2002.
3. Villegas, D.; Van Damme, M.; Venderborght, B.; Beyl, P.; Lefeber, D. Third-generation pleated pneumatic articial muscles for robotic applications: Development and comparision with mckibben muscle. *Adv. Robot.* **2012**, *26*, 1205–1227. [CrossRef]
4. Tondu, B.; Lopez, P. Modeling and control of McKibben artificial muscle robot actuators. *IEEE Control Syst. Mag.* **2000**, *20*, 15–38.
5. Situm, Z.; Herceg, S. Design and control of a manipulator arm driven by pneumatic muscle actuators. In Proceedings of the 16th Mediterranean Conference on Control and Automation, Ajaccio, France, 25–27 June 2008; pp. 926–931. [CrossRef]
6. Jobbagy, B.; Simsik, D.; Karch, J.; Onofrejova, D. Robotic Arm with Artificial Muscles in Rehabilitation. *Procedia Eng.* **2014**, *96*, 195–202. [CrossRef]
7. Mohannad, F.; Norsinnira, Z.A.; Mohammed, H.A. Development of anthropomorphic robotic hand driven by Pneumatic Artificial Muscles for robotic applications. *IOP Conf. Ser. Mater. Sci. Eng.* **2018**, *342*, 012052.
8. Mazzolai, B.; Margheri, L.; Cianchetti, M.; Dario, P.; Laschi, C. Soft-robotic arm inspired by the octopus: II. From artificial requirements to innovative technological solutions. *Bioinspir. Biomim.* **2012**, *7*, 025005. [CrossRef] [PubMed]
9. Liu, Y.; Zang, X.; Liu, X.; Wang, L. Design of a biped robot actuated by pneumatic artificial muscles. *Bio-Med. Mater. Eng.* **2015**, *26*, 757–766. [CrossRef]
10. Sekine, M.; Shiota, K.; Kita, K.; Namiki, A.; Yu, W. A lightweight shoulder prosthesis with antagonistic impact-absorbing hybrid actuation for bimanual activities of daily living. *Adv. Mech. Eng.* **2016**, *8*, 1–17. [CrossRef]
11. Sawicki, G.S.; Ferris, D.P. A pneumatically powered knee-ankle-foot orthosis (KAFO) with myoelectric activation and inhibition. *J. Neuroeng. Rehabil.* **2009**, *6*, 23. [CrossRef] [PubMed]
12. Aun, K.K.; Anh, H.P.H. System modeling identification and control of the two-link pneumatic artificial muscle manipulator optimized with genetic algorithms. In Proceedings of the 2007 IEEE International Conference on Control and Automation (ICCA), Guangzhou, China, 30 May–1 June 2007; pp. 501–506.
13. Walker, I.D. Continuous backbone "continuum" robot manipulators. *ISRN Robot.* **2013**, *2013*, 726506. [CrossRef]
14. Bosnjak, N.; Wang, S.; Han, D.; Lee, H.; Chester, S.A. Modeling of fiberreinforced polymeric gels. *Mech. Res. Commun.* **2019**, *96*, 7–18. [CrossRef]
15. Wang, S.; Chester, S.A. Experimental characterization and continuum modeling of inelasticity in filled rubber-like materials. *Int. J. Solids Struct.* **2018**, *136*, 125–136. [CrossRef]
16. Wang, S.; Chester, S.A. Modeling thermal recovery of the mullins effect. *Mech. Mater.* **2018**, *126*, 88–98. [CrossRef]
17. Wang, S.; Decker, M.; Henann, D.L.; Chester, S.A. Modeling of dielectric viscoelastomers with application to electromechanical instabilities. *J. Mech. Phys. Solids* **2016**, *95*, 213–229. [CrossRef]
18. Gu, G.Y.; Li, C.X.; Zhu, L.M.; Su, C.Y. Modeling and identification of piezoelectric-actuated stages cascading hysteresis nonlinearity with linear dynamics. *IEEE/ASME Trans. Mechatron.* **2016**, *21*, 1792–1797. [CrossRef]
19. Ko, Y.R.; Hwang, Y.; Chae, M.; Kim, T.H. Direct identification of generalized Prandtl–Ishlinskii model inversion for asymmetric hysteresis compensation. *ISA Trans.* **2017**, *70*, 209–218. [CrossRef]
20. Janaideh, M.A.; Rakheja, S.; Su, C.Y. A generalized Prandtl–Ishlinskii model for characterizing the hysteresis and saturation nonlinearities of smart actuators. *Smart Mater. Struct.* **2009**, *18*, 045001. [CrossRef]
21. Wang, Y.F.; Xu, R.; Zhou, M.L. Prandtl-Ishlinskii modeling for giant magnetostrictive actuator based on internal time-delay recurrent neural network. *IEEE Trans. Magn.* **2018**, *54*, 1–4.
22. Wickramatunge, K.C.; Leephakpreeda, T. Study on mechanical behaviors of pneumatic artificial muscle. *Int. J. Eng. Sci.* **2010**, *48*, 188–198. [CrossRef]
23. Xie, S.L.; Liu, H.T.; Mei, J.P.; Gu, G.Y. Modeling and compensation of asymmetric hysteresis for pneumatic artificial muscles with a modified generalized Prandtl–Ishlinskii model. *Mechatronics* **2018**, *52*, 49–57. [CrossRef]
24. Lin, C.J.; Lin, C.R.; Yu, S.K.; Chen, C.T. Hysteresis modeling and tracking control for a dual pneumatic artificial muscle system using Prandtl–Ishlinskii model. *Mechatronics* **2015**, *28*, 35–45. [CrossRef]
25. Chou, C.P.; Hannaford, B. Measurement and modeling of McKibben pneumatic artificial muscles. *IEEE Trans. Robot. Autom.* **1996**, *12*, 90–102. [CrossRef]
26. Vo-Minh, T.; Tjahjowidodo, T.; Ramon, H.; Brussel, H.V. A New Approach to Modeling Hysteresis in a Pneumatic Artificial Muscle Using the Maxwell-Slip Model. *IEEE/ASME Trans. Mechatron.* **2011**, *16*, 177–186. [CrossRef]
27. Yu, X.W.; Yang, H.; Hao, L.N. Hysteresis modelling based on improved J-A model and compensation control for pneumatic muscle. *Chin. Hydraul. Pneum.* **2018**, *7*, 19–23.
28. Kosaki, T.; Sano, M. Control of a parallel manipulator driven by pneumatic muscle actuators based on a hysteresis model. *J. Environ. Eng.* **2011**, *6*, 316–327. [CrossRef]
29. Kosaki, T.; Minesaki, A.; Sano, M. Adaptive hysteresis compensation with a dynamic hysteresis model for control of a Pneumatic Muscle Actuator. *J. Environ. Eng.* **2012**, *7*, 53–65. [CrossRef]

30. Mei, J.; Xie, S.; Liu, H.; Zang, J. Hysteresis Modeling and Compensation of Pneumatic Artificial Muscles using the Generalized Prandtl-Ishlinskii Model. *Stroj. Vestn. J. Mech. Eng.* **2017**, *63*, 657–665.
31. Tondu, B. Modelling of the McKibben artificial muscle: A review. *J. Intell. Mater. Syst. Struct.* **2012**, *23*, 225–253. [CrossRef]
32. Daerden, F.; Lefeber, D. Pneumatic Artificial Muscles: Actuators for robotics and automation. *Eur. J. Mech. Environ. Eng.* **2002**, *47*, 10–21.
33. Reynolds, D.B.; Repperger, D.W.; Phillips, C.A.; Bandry, G. Modeling the dynamic characteristics of pneumatic muscle. *Ann. Biomed. Eng.* **2003**, *31*, 310–317. [CrossRef]
34. Cao, J.; Xie, S.Q.; Zhang, M.; Das, R. A new dynamic modelling algorithm for pneumatic muscle actuators. In *Intelligent Robotics and Applications*; Springer: Cham, Switzerland, 2014; pp. 432–440.
35. Cao, J.; Xie, S.Q.; Das, R. MIMO Sliding Mode Controller for Gait Exoskeleton Driven by Pneumatic Muscles. *IEEE Trans. Control Syst. Technol.* **2018**, *26*, 274–281. [CrossRef]
36. Kelasidi, E.; Andrikopoulos, G.; Nikolakopoulos, G.; Manesis, S. A survey on pneumatic muscle actuators modeling. In Proceedings of the 2011 IEEE International Symposium on Industrial Electronics (ISIE), Gdansk, Poland, 27–30 June 2011; pp. 1263–1269.
37. Al-Ibadi, A.; Nefti-Meziani, S.; Davis, S. Efficient Structure-Based Models for the McKibben Contraction Pneumatic Muscle Actuator: The Full Description of the Behaviour of the Contraction PMA. *Actuators* **2017**, *6*, 32. [CrossRef]
38. Filip, O.; Deaconescu, A.; Deaconescu, T. Experimental Research on the Hysteretic Behaviour of Pressurized Artificial Muscles Made from Elastomers with Aramid Fibre Insertions. *Actuators* **2020**, *9*, 83. [CrossRef]
39. Filip, O.; Deaconescu, A.; Deaconescu, T. Mechanical Design of a Bioinspired Compliant Robotic Wrist Rehabilitation Equipment. *Appl. Sci.* **2021**, *11*, 1246. [CrossRef]
40. Petre, I.; Deaconescu, A.; Rogozea, L.; Deaconescu, T. Orthopaedic Rehabilitation Device Actuated with Pneumatic Muscles. *Int. J. Adv. Robot. Syst.* **2014**, *11*, 105. [CrossRef]
41. Petre, I.; Deaconescu, A.; Sârbu, F.; Deaconescu, T. Pneumatic Muscle Actuated Wrist Rehabilitation Equipment Based on the Fin Ray Principle. *Stroj. Vestn. J. Mech. Eng.* **2018**, *64*, 383–392.